This is the final peer-reviewed accepted manuscript of:

G. Fontanesi, A. Guerra, F. Guidi, J. A. Vásquez-Peralvo, N. Shlezinger, A. Zanella, E. Lagunas, S. Chatzinotas, D. Dardari, P. M. Djurić, "A Deep-NN Beamforming Approach for Dual Function Radar Communication THz UAV," in IEEE Transactions on Vehicular Technology, 2024.

The file is available at:

https://doi.org/10.1109/TVT.2024.3453194

Terms of use:

Some rights reserved. The terms and conditions for the reuse of this version of the manuscript are specified in the publishing policy. For all terms of use and more information see the publisher's website.

A Deep-NN Beamforming Approach for Dual Function Radar-Communication THz UAV

Gianluca Fontanesi, *Member, IEEE* Anna Guerra, *Member, IEEE*, Francesco Guidi, *Member, IEEE*, Juan A. Vásquez-Peralvo, *Member, IEEE*, Nir Shlezinger, *Member, IEEE*, Alberto Zanella, *Senior Member, IEEE*, Eva Lagunas, *Senior Member, IEEE*, Symeon Chatzinotas, *Fellow, IEEE*, Davide Dardari, *Senior Member, IEEE*, and Petar M. Djurić, *Life Fellow, IEEE*

***Abstract*—In this paper, we consider a scenario with one unmanned aerial vehicle (UAV) equipped with a uniform linear array (ULA), which sends combined information and sensing signals to communicate with multiple ground base stations (GBSs) and, at the same time, senses potential targets placed within an interested area on the ground. We aim to jointly design the transmit beamforming with the GBSs association to optimize communication performance while ensuring high sensing accuracy. We propose a predictive beamforming framework based on a dual deep neural network (DNN) solution to solve the formulated nonconvex optimization problem. A first DNN is trained to produce the required beamforming matrix for any point of the UAV flying area in a reduced time compared to state-of-the-art beamforming optimizers. A second DNN is trained to learn the optimal mapping from the input features, power, and effective isotropic radiated power (EIRP) constraints to the GBSs association decision. Finally, we provide an extensive simulation analysis to corroborate the proposed approach and show the benefits of EIRP, Signal-to-Noise-plus-Interference Ratio (SINR) performance and computational speed.**

***Index Terms*—Unmanned aerial vehicle, ISAC, neural network, cellular network**

I. Introduction

WIRELESS communications and radio sensing are evolving towards the same technological solutions involving high frequencies, large antenna arrays, and miniaturized devices [1], [2]. Thereby, integrating sensing capabilities in wireless infrastructures offers new exciting opportunities for the next sixth generation (6G) cellular systems and beyond [3], [4]. However, sensing and communications have different roles: sensing collects and extracts information from noisy data, whereas communications are devoted to transmitting information through ad-hoc signaling schemes and recovering it from a noisy environment. The Integrated Sensing and Communication (ISAC) paradigm integrates both functionalities (e.g., by using the same hardware) to find a tradeoff between competing needs and mutual performance gains [5], [6].

G. Fontanesi was with the University of Luxembourg when the work was started and it is currently with Nokia Bell Labs, Germany {gianluca.fontanesi@nokia.com}.
J. Vásquez-Peralvo, E. Lagunas and S. Chatzinotas are with the University of Luxembourg {juan.vasquez, eva.lagunas,symeon.chatzinotas@uni.lu}.
A. Guerra, F. Guidi and A. Zanella are with the National Research Council of Italy ({anna.guerra, francesco.guidi, alberto.zanella}@cnr.it)
N. Shlezinger is with Ben Gurion University, Israel. (nirshl@bgu.ac.il).
D. Dardari is with WiLab-CNIT/DEI, University of Bologna, Italy. (davide.dardari@unibo.it).
P. M. Djurić is with the Stony Brook University, New York, USA. (petar.djuric@stonybrook.edu).

Several works have recently proposed different waveform designs to find the best sensing and communication tradeoffs. In [7], the authors consider the tradeoff between the detection probability and achievable rate for a joint communication and passive radar system. Then, [8] accounts for the tradeoff between estimation and communication and the design of a waveform favorable for target estimation and information delivery. Finally, in [9], the authors investigate the tradeoff arising in ISAC systems due to the different treatment of spatial degrees of freedoms (DOFs).

Waveform design is key in attaining integration gain and can be conceived either in a non-overlapping resource allocation scheme or in a fully unified framework [4]. In the first case, sensing and communications are split over orthogonal (non-overlapping) wireless resources [4], [10]. Differently, fully unified waveform design can follow two approaches: (1) a sensing-centric scheme when a typical sensing waveform (e.g., chirp signals) incorporates a communication functionality, e.g., [11], [12]; (2) a communication-centric scheme when a communication waveform (e.g., OFDM) is also used for sensing [13], and a joint design approach based on optimization [14]. New beamforming methods based on SF-RDA, FDA-MIMO have been proposed in [15], [16] to mitigate the problem of jammer.

Such a joint design is particularly appealing for networks of low-complexity devices, such as unmanned aerial vehicles (UAVs), as it allows the design of highly flexible and efficient systems overcoming the size, weight, and endurance constraints of autonomous agents [17], [18]. Indeed, towards the realization of 6G, UAVs have attracted significant interest thanks to their low cost and their flexibility, which let them be a suitable solution for both communication and sensing [19]–[22]. UAVs are emerging sensing technologies that, thanks to their flexibility and their possibility of keeping a privileged line-of-sight (LoS) point of view, are often used for localization and sensing in time-critical applications [23]–[26]. The advantages of using UAVs with ISAC are many, but at the extreme, one can find two significant aspects. On the one hand, the UAVs' 3D mobility allows dual function radar communication (DFRC) tasks to be performed in an optimized manner: an optimized UAVs trajectory can further increase the performance of the ISAC system. On the other hand, ISAC is an integrated solution that supports easy and low-complexity hardware deployment of onboard battery constraint agents that requires determining the best beamforming and waveform

design. ISAC enables sharing wireless infrastructure and RF hardware and constructing compact and lightweight wireless devices with both communications and sensing capabilities. This is particularly promising as power and battery-constrained UAVs could be deployed as airborne nodes to provide wireless sensing support from the sky in 5G and beyond cellular networks [18]. Potential applications range from law enforcement, precision agriculture, and 3D environmental mapping to search, rescue, and military operations. In this perspective, high-frequency technology, such as Terahertz (THz) and mm-Wave, has emerged as a promising solution for sensing [27], for UAV integration thanks to their ease of miniaturization [28], and for all the solutions that entail the convergence of communication, localization and sensing capabilities [29].

A. Related Works and Contributions

The ISAC theoretical framework has been recently applied to UAVs [30]–[38], which can be classified according to the UAV's trajectory constraints and goals. More specifically, [33], [35], [36] consider the energy consumption of the UAV during the trajectory while achieving the sensing performance gains. In [33], a rotatory-wing UAV transmits the ISAC signal during its flight to simultaneously provide downlink communication service to a ground user and sense a target. The trajectory design problem aims to determine the subsequent UAV waypoints, hover points, and flight speeds to maximize the average communication rate while minimizing the Cramer-Rao lower bound (CRLB) of the target location estimate. In [35], a ground base station (GBS) is deployed to deliver downlink wireless services to cellular users. A cellular-connected UAV equipped with a side-looking synthetic-aperture radar (SAR) flies and collects the echoes of communication signals originating from the GBS to sense objects and gain situational awareness. The UAV minimizes the overall propulsion energy consumption during the time horizon while maintaining acceptable sensing resolution by reusing cellular communication signals. In [36], the considered UAV is required to execute multiple sensing tasks in sequence within the cell coverage. Nevertheless, in [36], it has not been considered that, due to its high altitude, the UAV might associate with several candidates GBSs at different distances. Thus, the UAV-GBS association should be carefully considered when designing the UAV trajectory.

Other works as [30], [37], [39]–[42] focus on the UAV beamforming problem considering antenna arrays deployed on the UAV. The authors in [37], [39] consider a UAV equipped with a uniform linear array (ULA) to serve ground users and, simultaneously, to perform radar sensing towards potential ground targets. The objective is to maximize the average weighted sum-rate throughput by jointly optimizing the UAV trajectory, as well as the transmit information and sensing beamforming subject to the sensing requirements and transmit power constraints over different time slots.

In [30], the authors consider a UAV-ISAC system integrated with a ULA, to maximize the achievable rate, subject to the beam-pattern gain constraint and the maximum transmit power constraint. Works [40], [41] minimize a beampattern matching error by jointly optimizing the sensing and communication beamforming design subject to the transmit power constraints and secrecy rate [41] or transmit power and rate constraints [40]. The antenna pattern in these papers is the result of optimization solutions. However, these approaches make it difficult to simultaneously satisfy SLL, beamwidth, nulling, and EIRP constraints. This becomes even more complicated when a realistic high-gain sub-array is considered during the beam steering process.

In addition, the rotation of the antenna radiation pattern suffered by small/medium UAVs due to environmental factors has not yet been considered when considering the effectiveness of the proposed beamforming patterns.

These joint challenges introduce a high level of complexity. First, a realistic pattern synthesizer is complicated for the formed 3D beam based on a ULA in real-time ISAC application scenarios, especially in UAV-enabled ISAC networks where wireless links have diverse and varying elevation and azimuth angles. The complexity is even increased because the azimuth and elevation angles are not influenced for each trajectory point but are made from the rotation of the UAV and the applied GBS association policy.

This work aims to propose a deep neural network (DNN) solution that, together with the conventional challenges of ISAC, takes into account the UAV-GBS association problem described above, a realistic antenna beam pattern synthesizer and the possible rotation of the radiation pattern. To more efficiently exploit the benefits of beamforming in UAV-enabled ISAC networks, a more flexible antenna array, e.g., an ULA, is considered to form dedicated beams.

Thus, the main contributions of this manuscript can be summarized as follows:

- We consider a THz cellular-connected UAV system, required to communicate with surrounding GBSs and perform target sensing operation. Unlike previous works, we consider a realistic onboard UAV antenna design and beamforming, controlling the beam's position, the side lobe levels, and the nulling. In addition, we consider the rotation of the ULA antenna during the UAV trajectory.
- We formulate a novel UAV trajectory problem based on joint beamforming design and GBS association policy. The complexity of the proposed real-time antenna synthesizer, coupled with the nonconvex association constraints and UAV antenna rotation, makes the formulated problem nonconvex and high-dimensional. Consequently, conventional antenna synthesizers and mathematical approaches are inapplicable.
- We propose a double DNN based approach to approximate the non-linear mapping from the UAV position to the optimal beamforming weights selection and the optimal GBS selection. The labeled radio data for the first DNN is generated using an antenna pattern optimizer, which can synthesize a radiation pattern considering the beamwidth, pointing direction, and nulling as input data.
- With the advantage of reducing the time to generate the required beam, our DNN solution learns the directional beamforming weights for each UAV 's position in the flight area, including any effect on elevation and azimuth

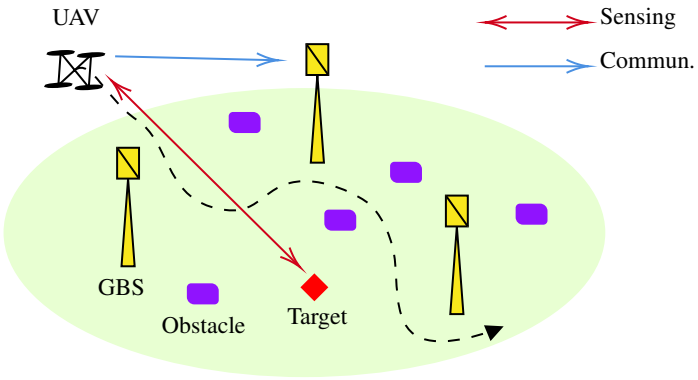

Fig. 1: Considered scenario, where the DFRC UAV needs to autonomously navigate the environment while guaranteeing reliable communication and sensing performance.

angle due to UAV rotation. In addition, a second DNN reduces the signaling overhead for the GBS-UAV association, indicating the best GBS association in terms of rate and minimum EIRP.

- We provide an extensive simulation analysis to corroborate the proposed framework and show its effectiveness in accuracy and speed compared to the antenna optimizer.

The rest of the paper is organized as follows: Sec. II introduces the system model of the DFRC UAV system. In Sec. III, we formulate the connectivity-constrained beam-pattern gain minimization problem, while Sec. IV details the proposed Neural Network (NN)-aided approach. Numerical results are reported in Sec. V, while Sec. VI provides concluding remarks.

A complete list of recent works on ISAC systems applied to UAV technology is reported in Table I.

II. System Model

We consider a cellular system, schematically depicted in Fig. 1, populated by a terrestrial network of GBSs and a UAV. More specifically, the UAV is required to act as a mobile DFRC system that simultaneously probes its surrounding environment through a monostatic radar while communicating with its associated GBS. We aim to facilitate the operation of such networks by adequately selecting the GBS and the choice of the suitable orientation and beam-pattern configuration for the UAV through an ad-hoc beam-pattern optimization technique to satisfy communication and sensing requirements.

Next, we first discuss the GBS association rule. After providing a brief overview of the considered geometry, we present the transmitted signal model and describe how we consider the signaling for sensing and communication, the ground-to-air channel, and finally, the received signal model.

A. GBS Association Policies

Selecting the best GBS to associate with is not trivial due to blockages, Non-Line of Sight (NLoS) links, or communication/sensing pointing angles that make the radiation pattern optimization unsuitable.

In particular, one can consider one of the following association approaches, defined also as policy in the results:

1) A possible association rule is represented by choosing the closest GBS. However, if the nearest-neighbor association is adopted, performance might degrade due to blockages. In addition, the communication and sensing angle might be very different.
2) A second possibility is to select the GBS with an azimuth angle close to the UAV-target azimuth angle to maximize the sensing performance.
3) A third possibility is to select the GBS experiencing the highest Signal-to-Noise-plus-Interference Ratio (SINR). This requires a complete scan of the environment to receive the GBS pilot information and, thus, higher overhead and latency. In addition, it might happen that the GBS with the highest SINR is not the one that allows optimizing the beam pattern for joint sensing and communication purposes.

As noted above, each approach has its challenges and limitations. Thus, we will investigate the performance of the three approaches for the system's joint sensing and communication performance.

B. System Geometry

The UAV mission period, namely $\mathcal{T} = [0, T]$ is discretized into N time slots, each with duration $\delta_t = T/N$. Here, δ_t is chosen to be sufficiently small so that the UAV location can be assumed to be approximately unchanged within each slot to facilitate the trajectory and beamforming design. In addition, we consider that the UAV aims to sense $U = 1$ target of interest at a known location $\mathbf{u}_0 = (x_0, y_0, z_0)$. At any time slot during the UAV trajectory, the UAV can associate only with one of the GBS.

We consider a 3D Cartesian system, represented in Fig. 2, where

- The location of the GBSs are fixed at $\mathbf{u}_k = (x_k, y_k, z_k), \quad k = 1, ..., K$ with K being the number of deployed GBSs, (x_k, y_k) denoting the location of the kth GBS and $z_k = h_{\text{BS}}$, $\forall k$;
- The time-varying location of the UAV at time slot $n \in \mathcal{N}$ is $\mathbf{q}(n) = (x(n), y(n), z(n))$. Then, consider the set of UAV trajectories as

$$\mathcal{Q} = \{\mathbf{q}_1, \ldots, \mathbf{q}_\ell, \ldots, \mathbf{q}_{N_\text{T}}\}, \tag{1}$$

where each trajectory can be expressed as a sequence of UAV positions

$$\mathbf{q}_\ell = \{\mathbf{q}_\ell(1), \ldots, \mathbf{q}_\ell(n), \ldots, \mathbf{q}_\ell(N)\}, \tag{2}$$

and N_T is the total number of flights performed by the UAV. We consider the initial and final positions being fixed, that is, $\mathbf{q}_\ell(1) = \mathbf{q}_\text{I}$, $\mathbf{q}_\ell(N) = \mathbf{q}_\text{F}$, $\forall \ell$.
- The UAV speed is fixed and upper limited by $\|\mathbf{q}(n+1) - \mathbf{q}(n)\| \leq \delta_t V_{\max}$ with $V_{\max}$ being the maximum speed.

The UAV is equipped with an array of M antennas whose coordinates are

$$\mathbf{p}_m = \mathbf{q}(n) + (x_m, y_m, z_m) = \mathbf{q}(n) + \mathbf{R}(\alpha, \beta, \gamma)\, \mathbf{p}_m^{(0)}, \tag{3}$$

Ref.	ISAC	UAV Role	Optimization Goal	Constraints	Opt. Technique
[33]	No	UAV-BS	Communication Rate, CRB	Energy, UAV mobility	Iterative Algorithm
[35]	Yes	UAV-UE	Tx Power, Range Resolution	Overall propulsion energy consumption	BCD
[37]	Yes	UAV-BS	Comm. Rate	Sensing Beam-Pattern Gain, UAV TX Power	SCA, SDR
[36]	No	UAV-UE	Tx Power, UAV speed	Velocity, acceleration, UAV Coverage, Sensing Rate	Problem decomposition
[39]	Yes	UAV-BS	Comm. Rate	Sensing Beam-Pattern Gain, UAV TX Power	CVX
[30]	Yes	UAV-BS	Communication Rate	Beam-Pattern Gain, max Transmit Power	SDR, eigenvalue decomposition
[40]	Yes	/	Beampattern error	Transmit Power, Rate	SDR
[41]	Yes	/	Beampattern error	Transmit Power, Secrecy Rate	SDR
This work	Yes	UAV-BS/UE	Beampattern error	Transmit Power, GBS Connectivity	DNN

TABLE I: Related works on UAV-ISAC systems.

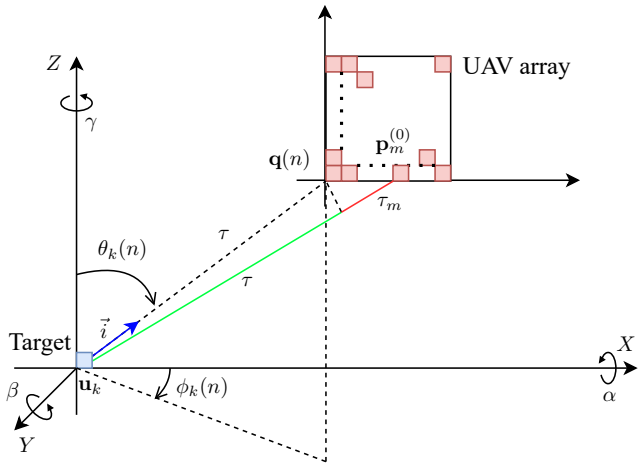

Fig. 2: System scenario and geometry.

where $\mathbf{q}(n)$ are the coordinates of the reference antenna and $m \in \{0, 1, \ldots, M-1\}$, and where

$$\mathbf{R}(\alpha, \beta, \gamma) = \mathbf{R}_x(\alpha)\mathbf{R}_y(\beta)\mathbf{R}_z(\gamma) \tag{4}$$

is a generic 3D rotation matrix with (α, β, γ) being the rotational angles around the x, y, and z axis respectively, and $\mathbf{p}_m^{(0)}$ is the antenna array position before the rotation. The definition of the rotation matrices $\mathbf{R}_x(\alpha)\mathbf{R}_y(\beta)\mathbf{R}_z(\gamma)$ is defined in [43], [44, 3.42] and it is reported in (5). Note that the orientation is affected by the trajectory only and not by speed variation, which we leave for future work. Consequently, it is straightforward to find the relationships in (6) between the coordinates of the antenna elements and the rotational angles.

Note that eq. (3) can specialize in different array geometries. In this work, we consider the UAV equipped with a squared Uniform Planar Square Array (UPA) with M antennas, initially distributed along the XZ-plane, such that it holds

$$\mathbf{p}_m^{(0)} = (x_m, y_m, z_m) = \left(m_x \frac{\lambda}{2}, 0, m_z \frac{\lambda}{2}\right), \tag{9}$$

where

$$m_x = \left(1 + \left\lfloor \frac{m}{\sqrt{M}} \right\rfloor\right) \frac{\lambda}{2},$$
$$m_z = \left[1 + (m \mod \sqrt{M})\right] \frac{\lambda}{2}$$

and we have assumed that the inter-antenna spacing is $d_{\text{ant}} = \frac{\lambda}{2}$ with λ being the carrier wavelength. In the sequel, we consider an optimization problem to control the array orientation using the rotational operation defined by (3).

C. Transmitted Signal Model

As highlighted in Fig. 3, we account for a DFRC system with separate waveforms for implementation simplicity rather than methods based on dual-function waveforms. With that said, let $\mathbf{s}(n)$ be a $(K+1)\times 1$ vector containing the transmitted waveforms as

$$\mathbf{s}(n) = [\underbrace{s_0(n)}_{\text{Sensing}}, \underbrace{s_1(n), \ldots, s_k(n), \ldots, s_K(n)}_{\text{Communication}}]^T, \tag{10}$$

where $s_k(n)$ represents the transmitted signal from the UAV to the k-th GBS at time slot n, whereas $s_0(n)$ represents the transmitted signal for sensing during the same time slot.

After the GBS selection, the UAV is attached to a single GBS, and (10) reduces to

$$\mathbf{s}(n) = [s_0(n), s_{\hat{k}_n}(n)]^T \in \mathcal{C}^{2\times 1}, \tag{11}$$

where $\hat{k}_n$ is the chosen GBS at time instant n.

We consider the UAV applying beamforming techniques for communications and sensing. We denote with $\mathbf{W}(n)$ the beamforming matrix given by

$$\mathbf{W}(n) = [\underbrace{\mathbf{w}_0(n)}_{\text{Sensing}}, \underbrace{\mathbf{w}_{\hat{k}_n}(n)}_{\text{Comm.}}] \in \mathcal{C}^{M\times 2} \tag{12}$$

with $\mathbf{w}_{\hat{k}_n}(n) \in \mathcal{C}^{M\times 1}$ representing the corresponding transmit beamforming vector to the GBS, whereas $\mathbf{w}_0(n)$ is the beamforming vector used for sensing. The generic beamforming vector, for $i \in \mathcal{I} = \{0, \hat{k}_n\}$, is given by

$$\mathbf{w}_i(n) = [e^{\jmath\varphi_{i,0}}, \ldots, e^{\jmath\varphi_{i,m}}, \ldots, e^{\jmath\varphi_{i,M-1}}]^T \in \mathcal{C}^{M\times 1}, \tag{13}$$

where $\varphi_{i,m}$ is the phase at the m-th antenna of the UAV array and M is the total number of antennas.

Accordingly, the transmitted signal from the UAV to the ith destination, GBS or target, is

$$\mathbf{x}_i(n) = \mathbf{w}_i(n)s_i(n) \in \mathcal{C}^{M\times 1}, \quad i \in \mathcal{I} = \left\{0, \hat{k}_n\right\}, \tag{14}$$

and the total transmitted signal per antenna is, as for Fig. 3

$$\mathbf{x}(n) = \mathbf{w}_0(n)s_0(n) + \mathbf{w}_{\hat{k}_n}(n)s_{\hat{k}_n}(n). \tag{15}$$

$$\mathbf{R}(\alpha,\beta,\gamma)=\begin{bmatrix}\cos(\alpha)\cos(\beta) & \cos(\alpha)\sin(\beta)\sin(\gamma)-\sin(\alpha)\cos(\gamma) & \cos(\alpha)\sin(\beta)\cos(\gamma)+\sin(\alpha)\sin(\gamma)\\ \sin(\alpha)\cos(\beta) & \sin(\alpha)\sin(\beta)\sin(\gamma)+\cos(\alpha)\cos(\gamma) & \sin(\alpha)\sin(\beta)\cos(\gamma)-\cos(\alpha)\sin(\gamma)\\ -\sin(\beta) & \cos(\beta)\sin(\gamma) & \cos(\beta)\cos(\gamma)\end{bmatrix}, \quad (5)$$

$$x_m = x_m^{(0)}\cos(\alpha)\cos(\beta)+y_m^{(0)}\left[\cos(\alpha)\sin(\beta)\sin(\gamma)-\sin(\alpha)\cos(\gamma)\right]+z_m^{(0)}[\cos(\alpha)\sin(\beta)\cos(\gamma)+\sin(\alpha)\sin(\gamma)], \quad (6)$$

$$y_m = x_m^{(0)}\sin(\alpha)\cos(\beta)+y_m^{(0)}\left[\sin(\alpha)\sin(\beta)\sin(\gamma)+\cos(\alpha)\cos(\gamma)\right]+z_m^{(0)}\left[\sin(\alpha)\sin(\beta)\cos(\gamma)-\cos(\alpha)\sin(\gamma)\right], \quad (7)$$

$$z_m = -x_m^{(0)}\sin(\beta)+y_m^{(0)}\cos(\beta)\sin(\gamma)+z_m^{(0)}\cos(\beta)\cos(\gamma). \quad (8)$$

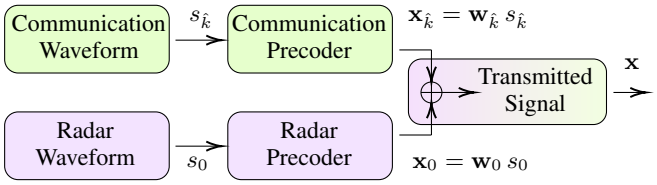

Fig. 3: Beamforming transmission for both communication and sensing.

The transmitted power is thus given by

$$\mathbb{E}\left[\mathbf{x}(n)^H\mathbf{x}(n)\right]=\mathbf{w}_0(n)^H\mathbb{E}\left[s_0(n)^H s_0(n)\right]\mathbf{w}_0(n) + \mathbf{w}_{\hat{k}_n}(n)^H\mathbb{E}\left[s_{\hat{k}_n}(n)^H s_{\hat{k}_n}(n)\right]\mathbf{w}_{\hat{k}_n}(n), \quad (16)$$

where $(\cdot)^H$ is the Hermitian operator and where we have assumed $\mathbb{E}\left[s_0(n)^H s_{\hat{k}_n}(n)\right]=0$ (orthogonality) [40]. Then, by further assuming

$$\mathbb{E}\left[s_{\hat{k}_n}(n)^H s_{\hat{k}_n}(n)\right]=1,\quad \mathbb{E}\left[s_0(n)^H s_0(n)\right]=1, \quad (17)$$

we can write

$$\mathbb{E}\left[\mathbf{x}(n)^H\mathbf{x}(n)\right]=\|\mathbf{w}_0(n)\|^2+\|\mathbf{w}_{\hat{k}_n}(n)\|^2. \quad (18)$$

Hence, according to (18), the constraint of the maximum available power can be expressed as

$$\|\mathbf{w}_0(n)\|^2+\|\mathbf{w}_{\hat{k}_n}(n)\|^2\le P_{\max}. \quad (19)$$

D. Air-to-Ground Channel Model

THz communication enables a high achievable rate thanks to the available bandwidth. However, the THz spectrum, lying in between microwaves and optical regions, suffers from high propagation losses and is sensitive to NLoS conditions. UAVs can have a privileged position in the 3D space and, thus, have a better chance of creating a LoS link with the intended target and GBS. Deploying high directive antennas with high directivity through large arrays on the UAV effectively mitigates the THz propagation losses [45].

This section characterizes the wireless channel between a possible destination, the selected GBSs or the target, and the UAV by deterministic large-scale path loss and random small-scale fading. As widely adopted in works dealing with UAV trajectory [36], we use a probabilistic path loss model, where the LoS and NLoS links are considered separately with different path loss exponents. Thus, two path loss functions can be described. We assume the signal through the THz band is affected by both free space loss and molecular absorption [46]. Then, to model the path loss of the LoS, we need to discriminate between two configurations, that is, $i=0$ (sensing) and $i=\hat{k}_n$ (communication).

In the sensing case, that is, when $i=0$, we can exploit the radar range equation to model the path loss as [47]

$$\mathsf{PL}_{\mathrm{LoS},0}(n)=\frac{\lambda^2}{(4\pi)^3\, d_0^4(n)}\rho_{\mathrm{T}}\cdot\exp\left(4K_{f_c}d_0(n)\right), \quad (20)$$

where the fourth power of the distance encapsulates the effect of the wave traveling the round-trip-channel between the target and the UAV, $d_0(n)$ is the UAV-target distance at time instant n, and ρ_{T} represents the target radar cross-section. Note that K_{f_c} represents the overall absorption coefficient of the transmission medium at the central (subcarrier) frequency f_c since, for THz-band signals, there is the molecular absorption caused by water vapor and other gases that increases the path loss. Thus, in the radar range equation, we have accounted twice for such an effect through the term $\exp\left(4K_{f_c}d_0(n)\right)$ [46].

For the communication case, that is, when $i=\hat{k}_n$, again, the main component is dictated by the free space loss, whose path loss can be calculated as [46]

$$\mathsf{PL}_{\mathrm{LoS},\hat{k}_n}(n)=\frac{\lambda^2}{(4\pi\, d_{\hat{k}_n}(n))^2}\exp\left(2K_{f_c}d_{\hat{k}_n}(n)\right). \quad (21)$$

The respective path loss in NLOS can be defined as [46]

$$\mathsf{PL}_{\mathrm{NLoS},\hat{k}_n}(n)=\mathsf{PL}_{\mathrm{LoS},\hat{k}_n}(n)\,K_N^2 =\frac{\lambda^2}{\left(4\pi d_{\hat{k}_n}(n)\right)^2}K_N^2\exp\left(2K_{f_c}d_{\hat{k}_n}(n)\right), \quad (22)$$

where K_N is the NLoS attenuation-loss coefficient.

It follows that at time slot n, the path loss between the UAV and the ith destination can be written as

$$\mathsf{PL}_i(n)=\mathbb{P}_{\mathrm{LoS},i}(n)\,\mathsf{PL}_{\mathrm{LoS},i}(n)+\mathbb{P}_{\mathrm{NLoS},i}(n)\,\mathsf{PL}_{\mathrm{NLoS},i}(n), \quad (23)$$

where $\mathbb{P}_{\mathrm{LoS},i}$ and $\mathbb{P}_{\mathrm{NLoS},i}$ are the probabilistic occurrences of the LoS and NLoS links, related to the ith destination, where $\mathbb{P}_{\mathrm{NLoS},i}=1-\mathbb{P}_{\mathrm{LoS},i}$.

We model the LoS probability between the UAV, of height $z(n)$, and the ith destination, of height z_i, as follows

$$\mathbb{P}_{\mathrm{LoS},i}(n) = - \kappa_1 \exp\left\{ - \kappa_2 \cdot \operatorname{atan}\left(\frac{z(n) - z_i}{d_i(n)\, \sin\left(\theta_i(n)\right)} \right) \right\} + \kappa_3, \quad (24)$$

where $d_i(n) = \|\mathbf{q}(n) - \mathbf{u}_i\|_2$ is the distance between the UAV and the destination whereas different values of κ_1, κ_2 and κ_3 lead to different propagation scenarios [48].

E. Received Signal Model

The steering vector $\mathbf{a}\left(\mathbf{q}(n), \mathbf{u}_i\right)$ towards the ith destination can be expressed as [43]

$$\mathbf{a}\left(\mathbf{q}(n), \mathbf{u}_i\right) = \left[e^{\jmath 2\,\pi\, f_c\, \tau_0}, \ldots, e^{\jmath 2\,\pi\, f_c\, \tau_m}, \ldots, e^{\jmath 2\,\pi\, f_c\, \tau_{M-1}}\right], \quad (25)$$

where f_c is the central frequency where the inter-antenna delay can be formulated as

$$\begin{aligned} \tau_m\left(\alpha, \beta, \gamma\right) &= \frac{1}{c}\, \mathbf{p}_m\, \vec{i}\left(\theta_k(n), \phi_k(n)\right) \\ &= \frac{1}{c}\, \left[x_m(\alpha, \beta, \gamma) \cos(\phi_k(n)) \sin(\theta_k(n)) + \right. \\ &\quad y_m(\alpha, \beta, \gamma) \sin(\phi_k(n)) \sin(\theta_k(n)) + \\ &\quad \left. z_m(\alpha, \beta, \gamma)\, \cos(\theta_k(n))\right], \end{aligned} \quad (26)$$

with $\mathbf{p}_m$ being the position coordinates of the mth array antenna, expressed in (3), and $\vec{i}\left(\theta_k(n), \phi_k(n)\right)$ being the wavefront direction.

As a result, the channel vector between the UAV and the ith destination can be written as the following $M \times 1$ vector:

$$\mathbf{h}_i(\mathbf{q}(n), \mathbf{u}_i) = \sqrt{\mathsf{PL}_i(n)}\, e^{\jmath 2\,\pi f_c \frac{d_i(n)}{c}}\, \mathbf{a}\left(\mathbf{q}(n), \mathbf{u}_i\right), \quad (27)$$

and the received signal at the ith destination can be written as

$$y_i(n) = \mathbf{h}_i^H(\mathbf{q}(n), \mathbf{u}_i)\mathbf{x}_i(n) + \nu_i(n) \in \mathcal{C}, \quad (28)$$

where $\nu_i(n)$ is the additive circular complex white Gaussian noise (AWGN) with variance σ^2.

Note that the time of arrival (TOA) between the mth antenna of the UAV and the ith destination at time n is approximated as

$$\tau_{m,i}\left(n\right) \approx \tau_m + \frac{\|\mathbf{u}_i - \mathbf{q}(n)\|}{c}, \quad (29)$$

where c is the speed of light and τ_m is the propagation time from the mth antenna to the array center located in $\mathbf{q}(n)$, as reported in Fig. 2.

Then, by defining the angles between the transmitter (UAV) and the receiver (GBS) as

$$\theta_i = \operatorname{acos}\left(\frac{z(n) - z_i}{d_i\left(n\right)} \right), \quad (30)$$

$$\phi_i(n) = \operatorname{atan}\left(\frac{y(n) - y_i}{x(n) - x_i} \right), \quad (31)$$

with $d_i\left(n\right) = \|\mathbf{u}_i - \mathbf{q}(n)\|$, and the direction vector as

$$\begin{aligned} \vec{i}\left(\theta, \phi\right) = &[\cos(\phi) \sin(\theta), \\ &\sin(\phi) \sin(\theta), \\ &\cos(\theta)]\,. \end{aligned} \quad (32)$$

Note that this TOA depends on the antenna array coordinates and the rotational angles (to be optimized). Indeed, the DFRC UAV can adapt its beamforming weights and orientation according to communication purposes, to the GBS association introduced in Section II-A, and sensing needs. The next section proposes the joint sensing and ground GBS association problem.

III. Problem Formulation

This section illustrates the joint optimization problem for balancing and finding a tradeoff between communications and sensing needs. Before presenting the problem, we separately introduce the metric functions to be optimized for both functionalities.

a) Communication metric: For enhancing the communications between the UAV and the selected GBS, we consider the SINR at the $\hat{k}_n$-th GBS formulated as

$$\mathsf{SINR}(\mathbf{q}(n), \mathbf{u}_{\hat{k}_n}) = \frac{|\mathbf{h}_{\hat{k}_n}^H(\mathbf{q}(n), \mathbf{u}_{\hat{k}_n})\mathbf{w}_{\hat{k}_n}(n)|^2}{\sigma^2 + |\mathbf{h}_0^H(\mathbf{q}(n), \mathbf{u}_0)\mathbf{w}_0(n)|^2}. \quad (33)$$

We have considered the worst-case scenario where the receiver cannot cancel the radar signals' interference before decoding its desirable information signal [40].

b) Sensing metric: A key performance metric adopted in literature for radar signal design is the transmit beam-pattern [49], [50]. The transmit beam pattern describes the transmit signal power at a generic focal point pointed towards the potential target in the interested area. Without prior knowledge of the target location, the transmit signal power is pointed at any value in the range $[-\pi/2, \pi/2]$ to perform a target search in any direction. Here, we assume the target is fixed in one position and that the position is known a priori. In the following, we note the estimated position of the target as $\hat{\mathbf{u}}_0$.

Starting from [50], we can formalize the transmit beam-pattern gain towards location $\mathbf{u}_0$ as

$$\begin{aligned} &B(\mathbf{q}(n), \mathbf{u}_0) = \\ &\left(\mathbf{a}\left(\mathbf{q}(n), \mathbf{u}_0\right)\right)^H (\|\mathbf{w}_0(n)\|^2 + \|\mathbf{w}_{\hat{k}_n}(n)\|^2) \mathbf{a}\left(\mathbf{q}(n), \mathbf{u}_0\right). \end{aligned} \quad (34)$$

We highlight that on the one hand, $\mathbf{a}(\mathbf{q}(n), \mathbf{u}_0)$ is a known function of θ since we initially assume a single static target, such that $j = 1, u_1 = (x_1, y_1, z_1)$. On the other hand, the beam pattern B varies along the trajectory because we assume that the angle between the target and the UAV changes through time.

Then, let $B^\star(\mathbf{q}_\ell(n), \mathbf{u}_i)$ denote the desired beam pattern, which specifies the desired beamforming weights and directions for the N UAV positions along the ℓth trajectory.

We can then formalize a cost function C that defines the beam-pattern matching error along the ℓth trajectory as

$$C(\mathbf{q}_\ell(n), \mathbf{W}_\ell(n)) = \sum_{\forall \ell, n=1}^{N} |B^\star(\mathbf{q}_\ell(n), \mathbf{u}_0) - B(\mathbf{q}_\ell(n), \mathbf{u}_0)|^2, \quad (35)$$

where we added subscript ℓ to $\mathbf{W}$ to indicate the beamforming matrix associate to the ℓ-trajectory.

We note that, according to (34), we would like to choose R_d and $\mathbf{w}_{\hat{k}_n}$ under the total transmit power constraint such that the available transmit power is used to maximize the signal power at the locations of interest.

c) Problem formulation: Our objective is to minimize the beam-pattern gain error, expressed in (35) optimizing R_d and $\mathbf{w}_{\hat{k}_n}$ together with the optimal GBS $\hat{k}_n$, subject to a connectivity constraint. Thus, our optimization problem can be formulated as

$$\mathcal{P}: \min_{\mathbf{o},\mathbf{W}_\ell,\hat{k}_n} \quad C(\mathbf{q}_\ell, \mathbf{W}_\ell(n)) \tag{36a}$$

$$\text{s.t.} \quad z(n) > z_{\hat{k}_n} = h_{\text{BS}}, \tag{36b}$$

$$\mathbf{q}(1) = \mathbf{q}_{\text{I}}, \mathbf{q}(N) = \mathbf{q}_{\text{F}} \tag{36c}$$

$$\|\mathbf{w}_0(n)\|^2 + \|\mathbf{w}_{\hat{k}_n}(n)\|^2 \leq P_{\max}, \tag{36d}$$

$$\mathsf{SINR}(\mathbf{q}(n), \mathbf{u}_{\hat{k}_n}) \geq \gamma_{\text{SINR}}. \tag{36e}$$

where $\mathbf{o} = [\alpha, \beta, \gamma]$, (36b) ensures the UAV height respects the local height regulations, with h_{BS} indicating the minimum required height; (36c) guarantees that the UAV starts and ends its trajectory at the required locations. Then, (36d) denotes the power constraint on the UAV, with $P_{\max}$ denoting the maximum tolerable transmitted power. Finally, (36e) ensures the minimum connectivity constraint with the GBS.

Note that, in general, it is difficult optimally solve problem $\mathcal{P}$ for the following reasons:

- The cost function is not convex. To make it convex, an auxiliary variable should be introduced [49]. However, this would add another constraint to the problem, increasing the complexity.
- Even if the objective cost function can be turned into a linear function, modeling the end-to-end channel of UAV-Base Station (BS) to derive (36e) requires accurate channel modeling and perfect global channel information. This might be complicated or even impractical for the THz frequency band under consideration.
- The formulated problem requires a joint solution for the sensing and the GBS association problem. A conventional approach would lead to splitting the solution into two problems and operate an alternate optimization approach while we propose a unique solution.
- Lastly, due to the sharp LoS/NLoS transitions, the convex shaped GBS coverage property may not hold [51]

Consequently, in the next section, we propose a double DNN approach.

IV. Proposed DNN Approach

We propose a data-driven approach to develop a learning-based beamforming scheme to address problem $\mathcal{P}$. To this purpose, we note that (36) can be considered as a beamforming design problem for each UAV 's position along the trajectory $\mathbf{q}_\ell$. Notably, the control of the constraints in (36) and the UAV rotation while finding the beamforming matrix is a complex task and requires synthesizing real-world, real-time beamforming patterns for any possible UAV trajectory point.

Currently developed ad-hoc tools, like beam-pattern optimizers [52], allow to manage for a single point at a time the different requirements of the beamforming applied at the DFRC UAV. For this reason, we compute training beamforming matrices for a different set of UAV trajectories that satisfy conditions (36b), (36c), (36d) using a beam-pattern optimizer. Then, we develop a DNN that synthesizes real-time realistic antenna beam patterns considering the radiation pattern's possible rotation.

The developed predictive beamforming framework is illustrated in Fig. 4 and consists of two phases: a) training with a Beam-Pattern Optimizer and b) a double DNN solution. We will describe in what follows the two phases separately.

Algorithm 1: Beam-Pattern Optimizer

Input: Initial UAV location;
EIRP*, EIRP per beam,;
$\text{SLL}_{\min}$, SLL minimum per beam;
$(\theta_{\text{Null}}, \phi_{\text{Null}})$, Null position per beam;
Output: $\mathbf{W}_{gv}$, Weight matrix based on previous inputs;
Data: Set of possible configurations on UAV considering system constraints;
$F_1 =$ initial value;
Data: Beam-Pattern Optimizer;
while counter $<$ $\text{counter}_{\max}$ **do**
  Compute: $\mathbf{W}_{gv}$
  Compute: radiation pattern, $\text{SLL}_{\text{c}}^{(\text{e})}$, $\text{SLL}_{\text{c}}^{(\text{a})}$ and EIRP_{c};
  Compute: $F(Z_1(\mathbf{W}_{gv}) + Z_2(\mathbf{W}_{gv}))$;
  if $F < \eta$ **then**
    $\mathbf{W}^{\star}_{gv} = \mathbf{W}_{gv}$;
    saves the optimal matrix;
    break
  else
    counter $\leftarrow$ counter $+ 1$;
  end
  Optimize: g, v, $\text{SLL}^{(\text{a})}$, $\text{SLL}^{(\text{e})}$, and PPE;
end
Save the optimal matrix $\mathbf{W}_{gv}$;

A. Beam-Pattern Optimizer for Training Data Generation

During the first phase a), a beamforming matrix for a different set of UAV trajectories is created such that it satisfies conditions (36b), (36c), (36d).

We consider a realistic antenna and a realistic number of antenna elements to perform the communication and sensing task and compute the inherent footprint. Accordingly, we consider a patch antenna that generates a cardioid radiation pattern and a maximum number of $M = 100$ elements. The direction angles, measured in azimuth and elevation, are defined geometrically by the positions of the UAV, the associated GBS, and the target. According to the considerations above, the nulling operation has to be performed in the directions of the non-attached GBSs.

The beam-pattern optimizer operates by activating or deactivating the number of active rows (m_x) and columns (m_z) in the array and finding the proper tapering by selecting the adequate side lobe level (SLL) in both planes to generate the

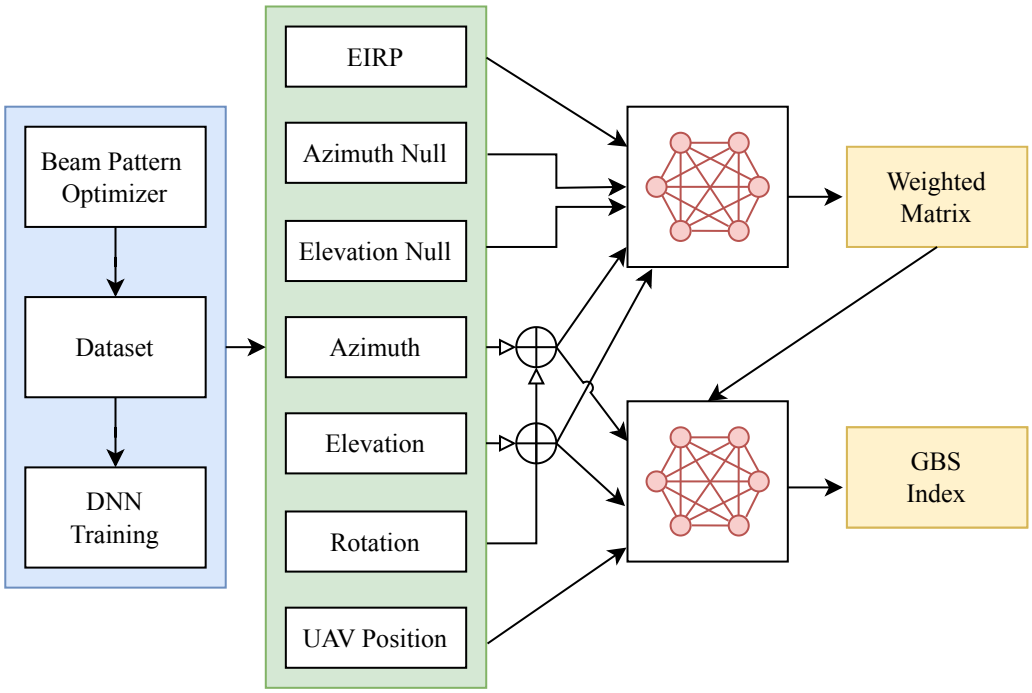

Fig. 4: Architecture and inputs/outputs of the proposed NN solution.

required $\theta_{3\text{dB}}$ in the elevation ($\theta^{(\text{e})}_{3\text{dB}}$) and azimuth planes ($\theta^{(\text{a})}_{3\text{dB}}$), and computing the required power per element to address the necessary effective isotropic radiated power (EIRP). For each position of the UAV, we have to compute two array weights vectors: (i) one dedicated to the sensing operation and (ii) one dedicated to the communication.

According to the previous considerations, the cost function is composed of the sum of two sub-objectives as follows

$$\mathbf{W}^{\star}_{gv} = \min_{\mathbf{W}_{gv}} \quad Z_1(\mathbf{W}_{gv}) + Z_2(\mathbf{W}_{gv}), \tag{37}$$

where $\mathbf{W}_{gv}$ indicates the gv-th element of the beamforming matrix, $Z_1(\mathbf{W}_{gv})$ and $Z_2(\mathbf{W}_{gv})$ are given by

$$\begin{cases} Z_1(\mathbf{W}_{gv}) = \left(\dfrac{|\text{SLL}^{(\text{a})}_{\text{c}}(\mathbf{W}_{gv}) - \text{SLL}^{(\text{a})}_{\text{o}}|}{\text{SLL}^{(\text{a})}_{\text{o}}} \right. \\ \qquad\qquad \left. + \dfrac{|\text{SLL}^{(\text{e})}_{\text{c}}(\mathbf{W}_{gv}) - \text{SLL}^{(\text{e})}_{\text{o}}|}{\text{SLL}^{(\text{e})}_{\text{o}}} \right) \cdot k_1 \\ Z_2(\mathbf{W}_{gv}) = \dfrac{\text{EIRP}(\mathbf{W}_{gv}) - \text{EIRP}^{*}}{\text{EIRP}^{*}} \cdot k_2 \,. \end{cases} \tag{38}$$

Note that $Z_1(\mathbf{W}_{gv})$ computes the error between the minimum desired SLL in both planes, that is, $\text{SLL}^{(\text{a})}_{\text{o}}, \text{SLL}^{(\text{e})}_{\text{o}}$ compared with their computed counterparts $\text{SLL}^{(\text{a})}_{\text{c}}, \text{SLL}^{(\text{e})}_{\text{c}}$ per beam. $Z_2(\mathbf{W}_{gv})$ reports the error between the desired EIRP^{*} and the calculated EIRP per beam. Each of those terms has a weighting factor k_1 and k_2 that will add additional importance to their calculation.

With that said, the algorithm operates as follows. First, it requires the azimuth and elevation coordinates of the center of the beam, the tolerable SLL range delimited by the minimum (SLL_{min}) values, the required EIRP (EIRP_{d}), and the null position ($\theta_{\text{Null}}, \phi_{\text{Null}}$). Then, the progressive phase shift, nulling, and tapering based on Chebyshev amplitude control are calculated and given as an initial weight matrix $\mathbf{W}_{gv}$ to the optimization algorithm with all the active elements and an initial power per element PPE. Later, the algorithm calculates, for each iteration, the radiation pattern principal cuts per beam and extracts the SLL, nulling, and EIRP for both cuts. Based on the previously extracted parameters, the algorithm calculates the cost function F, which, if it is lower than the minimum threshold, η, then the algorithm stops,

Parameters	*Value*	*Parameters*	*Value*
Area size	$2.25\,\text{km}^2$	BS height	2 m
Number of BS K	5	max EIRP	37 dBm
UAV height	100 m	Bandwidth	100 MHz
UAV speed	10m	Frequency	0.3 THz
δ_t	1 sec	Noise Power	-110 dBm
SNR threshold	0.3 dB	UAV training trajectories	100

TABLE II: Simulation Parameters

	SLL (dB)	EIRP (dBm)	ϕ_0 θ_0	ϕ_{target} θ_{target}	$\phi_{\text{Null},1}$ $\theta_{\text{Null},1}$	$\phi_{\text{Null},2}$ $\theta_{\text{Null},2}$
# 1	>15	15.38	43.6° 16.2°	48.54° 26.16°	12.61° 42.63°	76.64° 42.4°
# 2	>23	18	$-58.4°$ 8.4°	8.84° 11.26°	57.09° 25.47°	33.85° 27.30°

TABLE III: Input parameters for UAV trajectory point 1 (# 1) and 2 (# 2).

	SLL (dB)	EIRP (dBm)	Active elements
# 1	30.2	15.3801	100
# 2	25.6	18.001	100

TABLE IV: Output parameters of the radiation pattern presented in Fig. 5 for UAV Trajectory Point 1 (# 1) and 2 (# 2).

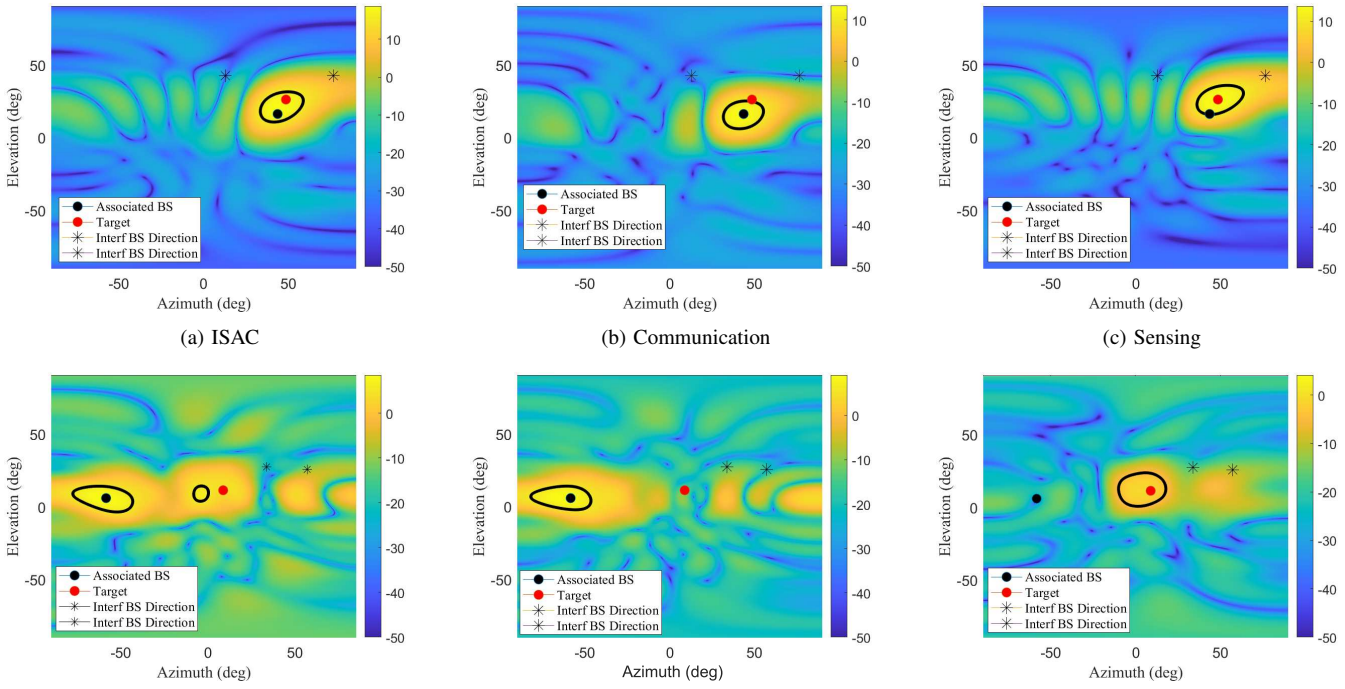

(a) ISAC (b) Communication (c) Sensing

(d) ISAC (e) Communication (f) Sensing

Fig. 5: Radiation patterns under different requirements in a case where the target and the associated BS positions are close (figures a-b-c) or far apart (figures d-e-f). The unit of the colormap is dB. The black circle indicates the main radiation lobe where most of the power is directed. The stars represent the positions of the neighbouring GBS. In the ISAC cases a) and d), the computed weights can focus the power on both the target (red dot) and the associated BS (black dot). In the communication and sensing case, on the other hand, the beam pattern is optimized for only one of the tasks, communicating with the associated GBS or sensing the target. This is particularly visible when the sensing target and the associated BS are located distant to each other (figures e-f), where the black circle contains either the black or the red dot.

and the optimum weight matrix $\mathbf{W}^{\star}_{gv} = \mathbf{W}_{gv}$ will be the output. Note that the threshold is selected to have a slight error between the optimized and required values. On the other hand, if the cost function is above the threshold, the algorithm increases the counter and searches for a suitable active number of rows g, columns v, a Chebyshev taper based on the SLL admissible range, and power per element PPE and repeat the previous calculation until it found the optimal weight matrix.

The main steps are reported in Algorithm 1.

B. Proposed NN Solution

Problem 36 is highly non-convex, includes a GBS association procedure not considered in the beampattern optimizer, and requires running a new simulation every time the UAV moves. Moreover, the UAV might take many trajectories and scan different GBSs associations. During the training process and the different GBS association along its trajectories, conditions (36d) and (36e) might be satisfied for the single communication or sensing task, but failed when considered jointly. Thus, the weight recalculations via a beam optimizer for each UAV position and GBS association would lead to lengthy procedures with high computational resources and power consumption. This is unsuitable due to the need for fast response of the UAV.

In this sense, phase b) comes to help first produce the required beamforming matrix for any point of the UAV flying area in a reduced time compared to the optimizer. Second, we also address the UAV-GBS association problem described in II-A with constraints (36d) (36e), exploiting the output of the first NN to train a DNN to learn the optimal mapping from the input features to the GBS association decision.

In our approach, the output of the beamformer optimizer is used to train the DNN accounting for both the sensing and communication performance. We exploit the ability of DNN to map the input-output of generic scenarios in a model-agnostic way [53]. The training phase consists of generating random trajectories in the considered area. For each point in the trajectory the antenna pattern optimizer generates training beamforming weights. The beamforming weights for communication and sensing are generated via the beampattern optimizer presented in the previous section and then used as input training of DNN. Once trained, the optimized beamforming weights $\mathbf{W}_{\ell}$ can be obtained from the DNN. Once this training phase is completed, the UAV is able to generate, in the inference step, a beamforming matrix for any point in the flight area under consideration in a reduced computation time. The power hungry training procedure can be performed offline and leave the inference only, less computational expensive, to be performed on board.

Then, we employ a feed forward neural network (FFNN) implementation, where we load as input for the communication beamforming weights for each UAV position and for all the trajectories, the azimuth, and elevation towards the associated GBS, the azimuth and elevation of the interfering GBS based

on the decided GBS association rule, and the EIRP (Fig. 4). To generate the sensing weights, we load to the FFNN with the azimuth and elevation towards the target position and the associated EIRP.

C. Proposed NN Complexity Analysis

The computational complexity of the proposed radiation pattern optimization algorithm is primarily influenced by the number of antenna elements received as input. This algorithm uses the AF (array factor) formula to estimate the approximate radiation pattern for subsequent calculations of beamwidth, SLL (side lobe level), nulls, and EIRP (effective isotropic radiated power). As the total number of antenna elements increases, the algorithm's runtime also increases due to the need for larger matrices and more multiplications involved in the array factor calculation.

The computational complexity of the proposed DNN algorithm can be analyzed in terms of multiplications of its main components. The computational complexity of a fully connected network is typically given by the multiplication of the parameters of each fully connected layer and depends on the number of features in the input vector and the number of neurons in the layer [54], $O(\zeta_i \zeta_n)$, where ζ_i is the number of features and ζ_n the number of neurons in the layer. Finally, the overall complexity is given by the sum of all layers of the DNN.

V. Numerical Evaluation

A. Scenario Definition

This section provides extensive simulation data to validate the proposed framework and evaluate system parameters' impact on sensing and communication performance. For the simulations, we consider an area of $1.5 \times 1.5\,\mathrm{km}^2$, where five GBS are distributed. The starting and final UAV path points are set respectively at $[0, 0]\,\mathrm{m}$, $[700, 800]\,\mathrm{m}$, and target location is at $[350, 400]\,\mathrm{m}$. For ease of illustration, the flight altitude is assumed to be fixed at 100 m during the path [1]. We have randomly generated $N_T = 100$ different trajectories between the starting and final points. A sub-THz downlink system is considered, operating at $0.3\,\mathrm{THz}$. Table III specifies the remaining simulation parameters.

B. Evaluation of the Proposed DNN solution

To validate and demonstrate the capabilities of the antenna pattern optimizer that creates the dataset and the proposed DNN solution, let us consider two example trajectory points where an UAV phased array generates a radiation pattern with the parameters presented in Table III. The antenna optimizer considers an array antenna to produce a beam synthesized with SLL, pointing angle, EIRP, and nulling as input. The above generated are computed for each point of the UAV trajectories as follows: the pointing angle is the angle pointing to the associated GBS or target, the nulling is the direction of the two closest neighboring GBS, the EIRP is the minimum EIRP to satisfy constraint 36e. The generated M proper complex

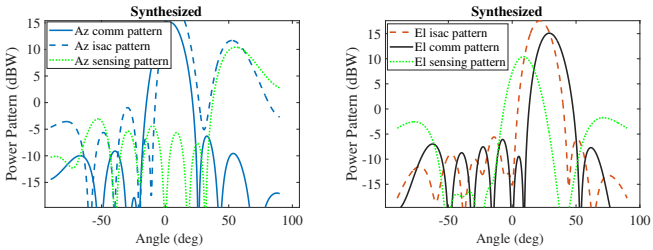

Fig. 6: Left: synthesized transmit azimuth beampattern profile. Right: synthesized transmit elevation beampattern profile.

Computational Time		
Solution	Training Epochs	Elapsed Time
Beamforming Optimizer	one UAV position	16 sec
Beamformer NN	200	47 sec - Training
Beamformer NN	1	60 msec - Inference
Association NN	200	20 sec - Training
Association NN	200	30 msec - Inference

TABLE V: Computation time for the DNN proposed solutions

weights $\mathbf{w}_m$, with $m \in \{1, ..., M\}$, are used to train the beamforming neural network. The beamforming network has an input layer of seven neurons corresponding to the desired bandwidth, sidelobes, power antenna constraints, one hidden layer (50 neurons), and an output layer (200 neurons). The proposed architecture task predicts the beamforming weights for each UAV position satisfying (36). The inputs are normalized to improve the optimization performance and the training process. We train the DNN by using the ADAM optimizer. We considered a slow learning rate and a batch size equal to 128. We chose a ratio of $70 - 30$ for the training and test sets. The structure of the association network is composed of an input layer with four neurons, corresponding to the UAV position in 2D space. Two hidden layers of 64 and 32 neurons follow, and finally, the output layer has one neuron corresponding to the BS index decision.

Fig. 5 shows the obtained (transmit) DNN beampattern gains in space at specifically chosen trajectory points for the sensing-only design, ISAC design, and the communication-only design, respectively. For ease of illustration, angle $(0, 0)$ and angles to the radar and GBS in azimuth and elevation are computed using the reference system in Fig. 2. The results show that the algorithm generates the three radiation patterns, addressing the desired EIRP and SLL requirements and pointing to the desired direction of the main beam and the nulls. For sensing design in Fig. 5c and Fig. 5f, the UAV is observed to direct its antenna main lobe ($\theta_{3\mathrm{dB}}$) at the center of the sensing area, and the sensing power exactly covers the whole sensing area, thanks to the adequately designed sensing beams in this case. Next, for the communication-only design in Fig. 5b and Fig. 5e, it is observed that the UAV antenna main lobe is deployed above the associating GBS, and the UAV 's transmission power is radiated towards GBS to perform the task of communication efficiently. Moreover, the beamforming nulls are placed in the neighboring GBS directions to minimize the interference at the GBS antenna side.

[1]Our proposed scheme can be extended to UAV paths with altitude variation.

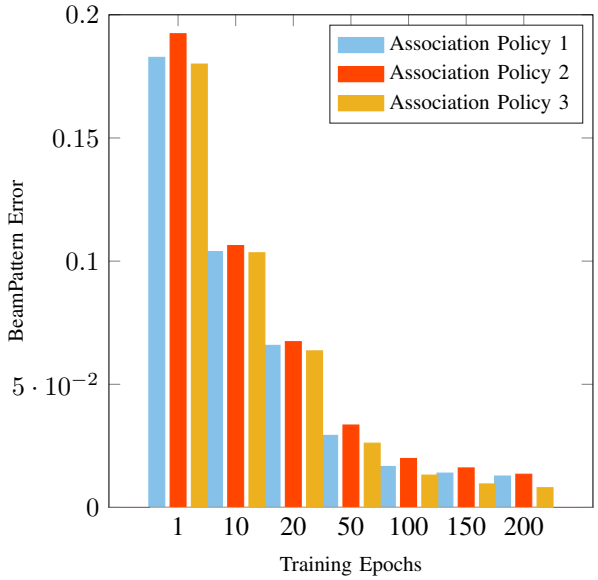

Fig. 7: Beam-pattern error vs training epoch for different GBS association policy.

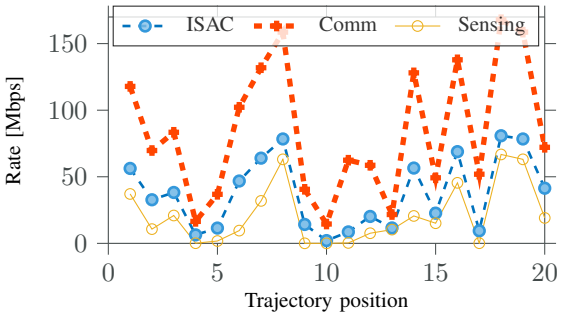

(a) Closest BS association strategy - Policy 1

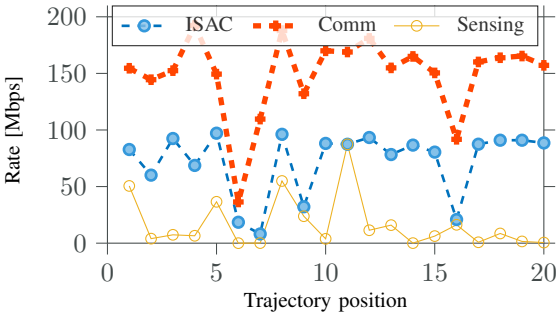

(b) Minimum angle association strategy - Policy 2

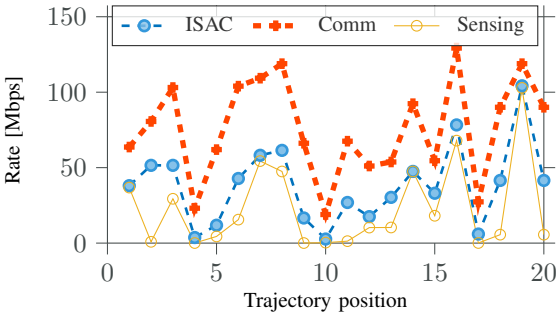

(c) Maximum RSSI association strategy - Policy 3

Fig. 8: Instantaneous rate under different requirements: sensing, communication, and ISAC

Finally, in Fig. 5a, Fig. 5d, it is observed that the UAV beamforming direction is deployed between the users and the sensing area. It is possible to note that when using the ISAC beamforming weights, the $\theta_{3\text{dB}}$ is directed towards the associated GBS. Two nulls are placed in the direction of inferring GBS. On the other hand, when using the sensing weights, the main lobe is directed towards the target while the GBS directions are not nulled properly. In this regard, Table IV shows the obtained SLL, EIRP, and active elements of the desired array pattern at the UAV for the two considered points. Fig. 6-left shows the transmit beampattern obtained by the DNN beamformer. The dashed line specifies the ISAC azimuth profile obtained by summing the communication and the sensing profile. Its counterpart, the transmit beampattern obtained by the beamforming optimizer, is shown in Fig. 6-right. The dashed line specifies the ISAC azimuth profile obtained by summing the communication and the sensing profile. It is observed that for the communication case, the pattern is formed to meet the SINR requirements with minimum power, while, for the sensing case, the pattern is created such that the resultant matching error can be minimized.

The proposed DNN solution can predict the beamforming weights with a significantly reduced time compared to running the beampattern optimizer for any point of the possible UAV trajectories. The training length and time for the proposed model are reported in Table V.

Fig. 7 shows the beampattern error along the DNN training epochs. The beampattern error diminishes with increasing training epochs, showing a convergent learning process for all three association policies. It means a stable beampattern at the UAV antenna is learned.

C. GBS association policies evaluation

To assess the GBS association policy performance, we consider the approaches described in Sec. II-A. For the sake of clarity, we adopt the following notation:

- Policy 1 refers to choosing the closest GBS;
- Policy 2 refers to choosing the GBS with azimuth angle closest to the target;
- Policy 3 refers to choosing the GBS experiencing the highest SINR.

It is also interesting to discuss the instantaneous communication rates achieved by different users in Fig. 8. Results in Fig. 8 are coherent with what was found in Fig. 5 and Fig. 5f. The beampattern optimized for communication provides the highest instantaneous rate along the UAV trajectory, while the ISAC design can balance the tradeoff between communication and sensing performances.

However, evaluating the best GBS association policy includes the evaluation of the tradeoff between constraints 36d and 36e in the optimization problem. Condition 36d imposes to satisfy a maximum transmission power/EIRP at the antenna side to limit the energy consumed by the UAV. The EIRP, in turn, has to be high enough to satisfy the SINR condition 36e

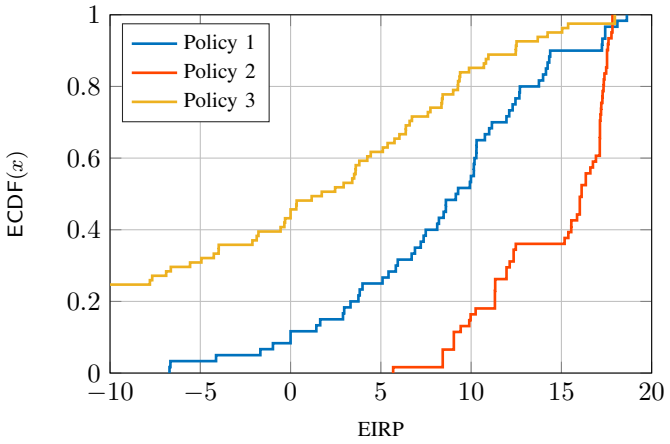

Fig. 9: Empirical cumulative distribution function (ECDF), indicated with $\mathsf{ECDF}(c)$, for the EIRP under different GBS association strategies.

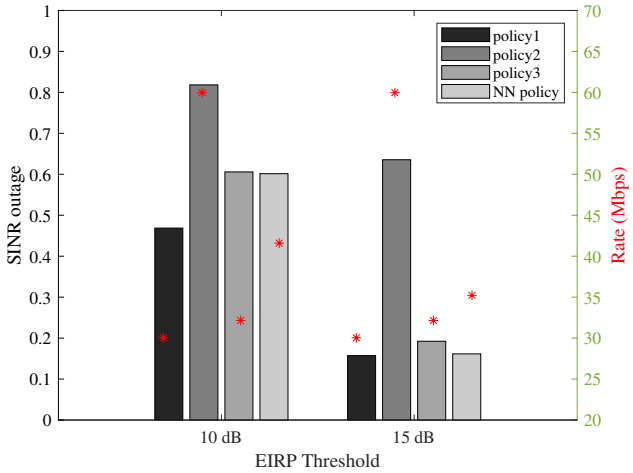

Fig. 10: SINR outage (gray bars) and communication average rate (red markers) for EIRP beampattern thresholds of $10\,\mathrm{dBm}$ and $15\,\mathrm{dBm}$.

at the GBS side to be able to decode the UAV signal. Fig. 9 shows the EIRP distribution during the UAV paths under the three different association strategies. While policy 2 helps to reach higher values of communication rate, policies 1 and 3 have lower EIRP values, leading to less power dissipation at the UAV antenna side.

Fig. 10 shows the average SINR outage at the UAV versus the achievable rate, comparing the three benchmark association policies and the proposed NN GBS association. The comparison is performed considering two different EIRP thresholds at the transmitter, 10 and $15\,\mathrm{dBm}$, respectively. Transmitting at the UAV with higher EIRP generally leads to lower SINR outage values. More specifically, compared to the Policy 1 and Policy 3 association strategies, the DNN-based association strategy leads to a better performance in terms of communication rate with a lower SINR outage. While Policy 2 can reach higher values of data rate, due to the high values of SINR outage, picking this policy would highly penalize the decoding of the signal reception at the GBS.

VI. Conclusions

In this paper, we proposed DNN solution for the joint ISAC beamforming and UAV-GBS association problem. The derived optimization problem accounts for UAV trajectory and orientation, sensing and communication beamforming weights, and GBS selection. Thus, the addressed optimization problem is comprehensive, considering various factors such as the trajectory and orientation of UAVs, beamforming weights for sensing and communication, and selecting suitable GBSs. Given the intricacies involved, particularly the nonconvex nature of the cost function and constraints, our approach leverages the power of two distinct DNNs. Our results demonstrate the considerable potential of our proposed approach in the context of UAV-enabled communication scenarios. Firstly, our solution showcases the capability to predict beamforming weights with significantly reduced computational time compared to state-of-the-art beampattern optimizers. Secondly, by utilizing a second DNN to determine the most suitable GBS association at each point along the UAV trajectory, our approach proves superior to traditional GBS association rules in terms of EIRP, SINR performance and computational speed. Future work includes comparing the proposed method with New beamforming methods based on SF-RDA, FDA-MIMO.

Acknowledgment

The work of G. Fontanesi, E. Lagunas, J. A. Vásquez-Peralvo and S. Chatzinotas was funded by the Luxembourg National Research Fund (FNR) under the project SmartSpace (C21/IS/16193290).

References

[1] W. Saad, M. Bennis, and M. Chen, "A vision of 6G wireless systems: Applications, trends, technologies, and open research problems," *IEEE Netw.*, vol. 34, no. 3, 2020.

[2] Z. Wei, F. Liu, C. Masouros, N. Su, and A. P. Petropulu, "Toward multi-functional 6G wireless networks: Integrating sensing, communication, and security," *IEEE Commun. Mag.*, vol. 60, no. 4, pp. 65–71, 2022.

[3] T. Wild, V. Braun, and H. Viswanathan, "Joint design of communication and sensing for beyond 5G and 6G systems," *IEEE Access*, vol. 9, pp. 30 845–30 857, 2021.

[4] F. Liu, Y. Cui, C. Masouros *et al.*, "Integrated sensing and communications: Towards dual-functional wireless networks for 6G and beyond," *IEEE J. Sel. Areas Commun.*, vol. 40, no. 6, pp. 1728–1767, 2022.

[5] A. R. Chiriyath, B. Paul, and D. W. Bliss, "Radar-communications convergence: Coexistence, cooperation, and co-design," *IEEE Trans. Cogn. Commun. Netw*, vol. 3, no. 1, pp. 1–12, 2017.

[6] F. Liu, C. Masouros, A. P. Petropulu, H. Griffiths, and L. Hanzo, "Joint radar and communication design: Applications, state-of-the-art, and the road ahead," *IEEE Trans. Commun.*, vol. 68, no. 6, pp. 3834–3862, 2020.

[7] B. K. Chalise, M. G. Amin, and B. Himed, "Performance tradeoff in a unified passive radar and communications system," *IEEE Signal Process. Lett.*, vol. 24, no. 9, pp. 1275–1279, 2017.

[8] B. K. Chalise and B. Himed, "Performance tradeoff in a unified multi-static passive radar and communication system," in *Proc. IEEE Radar Conf. (RadarConf18)*, 2018, pp. 0653–0658.

[9] F. Liu, Y.-F. Liu, A. Li, C. Masouros, and Y. C. Eldar, "Cramér-rao bound optimization for joint radar-communication beamforming," *IEEE Trans. Signal Process.*, vol. 70, pp. 240–253, 2021.

[10] D. Ma, N. Shlezinger, T. Huang, Y. Liu, and Y. C. Eldar, "Joint radar-communication strategies for autonomous vehicles: Combining two key automotive technologies," *IEEE Signal Process. Mag.*, vol. 37, no. 4, pp. 85–97, 2020.

[11] T. Huang, N. Shlezinger, X. Xu, Y. Liu, and Y. C. Eldar, "MAJoRCom: A dual-function radar communication system using index modulation," *IEEE J. Sel. Top. Signal Process*, vol. 68, pp. 3423–3438, 2020.

[12] D. Ma, N. Shlezinger, T. Huang, Y. Liu, and Y. C. Eldar, "FRaC: FMCW-based joint radar-communications system via index modulation," *IEEE J. Sel. Top. Signal Process*, vol. 15, no. 6, pp. 1348–1364, 2021.

[13] X. Chen, Z. Feng, Z. Wei, P. Zhang, and X. Yuan, "Code-division OFDM joint communication and sensing system for 6G machine-type communication," *IEEE Internet Things J.*, vol. 8, no. 15, pp. 12 093–12 105, 2021.

[14] J. Johnston, L. Venturino, E. Grossi, M. Lops, and X. Wang, "MIMO OFDM dual-function radar-communication under error rate and beampattern constraints," *IEEE J. Sel. Areas Commun.*, vol. 40, no. 6, pp. 1951–1964, 2022.

[15] L. Lan, J. Xu, G. Liao, S. Zhu, and H. C. So, "Mainlobe deceptive jammer suppression in sf-rda radar: Joint transmit-receive processing," *IEEE Transactions on Vehicular Technology*, vol. 71, no. 12, pp. 12 602–12 616, 2022.

[16] F. Wei, S. Zhu, L. Lan *et al.*, "Mainlobe deceptive jammer mitigation with subaperture-fda-mimo radar," *IEEE Transactions on Aerospace and Electronic Systems*, 2023.

[17] J. A. Zhang, F. Liu, C. Masouros *et al.*, "An overview of signal processing techniques for joint communication and radar sensing," *IEEE J. Sel. Topics Signal Process.*, 2021.

[18] Q. Wu, J. Xu, Y. Zeng *et al.*, "A comprehensive overview on 5G-and-beyond networks with UAVs: From communications to sensing and intelligence," *IEEE J. Sel. Areas in Commun.*, vol. 39, no. 10, pp. 2912–2945, 2021.

[19] A. Guerra, D. Dardari, and P. M. Djurić, "Dynamic Radar Network of UAVs: A Joint Navigation and Tracking Approach," *IEEE Access*, vol. 8, pp. 116 454–116 469, 2020.

[20] A. Merwaday and I. Guvenc, "UAV assisted heterogeneous networks for public safety communications," in *Proc. IEEE Wireless Commun. and Netw. Conf. Workshops (WCNCW)*, 2015, pp. 329–334.

[21] G. Fontanesi, A. Zhu, M. Arvaneh, and H. Ahmadi, "A transfer learning approach for UAV path design with connectivity outage constraint," *IEEE Internet Things J.*, pp. 1–1, 2023.

[22] A. Guerra, D. Dardari, and P. M. Djurić, "Dynamic Radar Networks of UAVs: A Tutorial Overview and Tracking Performance Comparison with Terrestrial Radar Networks," *IEEE Veh. Technol. Mag.*, vol. 15, no. 2, pp. 113–120, 2020.

[23] X. Wang, L. T. Yang, D. Meng *et al.*, "Multi-UAV cooperative localization for marine targets based on weighted subspace fitting in SAGIN environment," *IEEE Internet Things J.*, vol. 9, no. 8, pp. 5708–5718, 2021.

[24] A. Guerra, F. Guidi, D. Dardari, and P. M. Djurić, "Networks of UAVs of low complexity for time-critical localization," *IEEE Aerosp. Electron. Syst. Mag.*, vol. 37, no. 10, pp. 22–38, 2022.

[25] S. Zhang, R. Pöhlmann, T. Wiedemann *et al.*, "Self-aware swarm navigation in autonomous exploration missions," *Proc. IEEE*, vol. 108, no. 7, pp. 1168–1195, 2020.

[26] C. Wang, J. Wang, Y. Shen, and X. Zhang, "Autonomous navigation of UAVs in large-scale complex environments: A deep reinforcement learning approach," *IEEE Trans. Veh. Technol.*, vol. 68, no. 3, pp. 2124–2136, 2019.

[27] M. Lotti, G. Pasolini, A. Guerra *et al.*, "Radio SLAM for 6G systems at THz frequencies: Design and experimental validation," *IEEE J. Sel. Topics Signal Proc.*, vol. 17, no. 4, pp. 834–849, 2023.

[28] A. Guerra, F. Guidi, D. Dardari, and P. M. Djurić, "Real-time learning for THz radar mapping and UAV control," in *Proc. IEEE Int. Conf. on Autonomous Syst. (ICAS)*, 2021, pp. 1–5.

[29] H. Sarieddeen, N. Saeed, T. Y. Al-Naffouri, and M.-S. Alouini, "Next generation terahertz communications: A rendezvous of sensing, imaging, and localization," *IEEE Commun. Mag.*, vol. 58, no. 5, pp. 69–75, 2020.

[30] K. Meng, Q. Wu, S. Ma, W. Chen, and T. Q. Quek, "UAV Trajectory and Beamforming Optimization for Integrated Periodic Sensing and Communication," *IEEE Wireless Commun. Lett.*, vol. 11, no. 6, pp. 1211–1215, 2022.

[31] K. Meng, Q. Wu, S. Ma *et al.*, "Throughput maximization for UAV-enabled integrated periodic sensing and communication," *arXiv preprint arXiv:2203.06358*, 2022.

[32] K. Zhang and C. Shen, "UAV aided integrated sensing and communications," in *Proc. Veh. Techn. Conf. (VTC2021-Fall)*. IEEE, 2021, pp. 1–6.

[33] X. Jing, F. Liu, C. Masouros, and Y. Zeng, "Isac from the sky: Uav trajectory design for joint communication and target localization," *arXiv e-prints*, pp. arXiv–2207, 2022.

[34] M. Wang, P. Chen, Z. Cao, and Y. Chen, "Reinforcement learning-based UAVs resource allocation for integrated sensing and communication (isac) system," *Electronics*, vol. 11, no. 3, p. 441, 2022.

[35] S. Hu, X. Yuan, W. Ni, and X. Wang, "Trajectory planning of cellular-connected UAV for communication-assisted radar sensing," *IEEE Trans. Commun.*, 2022.

[36] S. Zhang, H. Zhang, B. Di, and L. Song, "Joint Trajectory and Power Optimization for UAV Sensing over Cellular Networks," *IEEE Commun. Letters*, vol. 22, no. 11, pp. 2382–2385, 2018.

[37] Z. Lyu, G. Zhu, and J. Xu, "Joint Trajectory and Beamforming Design for UAV-Enabled Integrated Sensing and Communication," in *Proc. IEEE Int. Conf. Commun (ICC)*. IEEE, 2022, pp. 1593–1598.

[38] J. Wu, W. Yuan, and L. Hanzo, "When uavs meet isac: Real-time trajectory design for secure communications," *IEEE Transactions on Vehicular Technology*, pp. 1–6, 2023.

[39] Z. Lyu, G. Zhu, and J. Xu, "Joint Maneuver and Beamforming Design for UAV-enabled Integrated Sensing and Communication," *arXiv preprint arXiv:2110.02857*, 2021.

[40] H. Hua, J. Xu, and T. X. Han, "Optimal Transmit Beamforming for Integrated Sensing and Communication," *IEEE Trans. Veh. Technol.*, vol. 72, no. 8, pp. 10 588–10 603, 2023.

[41] Z. Ren, L. Qiu, and J. Xu, "Optimal Transmit Beamforming for Secrecy Integrated Sensing and Communication," in *Proc. IEEE Int. Conf. on Commun.*, 2022, pp. 5555–5560.

[42] A. Guerra, F. Guidi, D. Dardari, and P. M. Djuric, "Reinforcement learning for joint detection & mapping using dynamic UAV networks," *IEEE Trans. Aerosp. Electron. Syst.*, To appear, 2023.

[43] A. Guerra, F. Guidi, and D. Dardari, "Single-Anchor Localization and Orientation Performance Limits Using Massive Arrays: MIMO vs. Beamforming," *IEEE Trans. Wireless Commun.*, vol. 17, no. 8, pp. 5241–5255, 2018.

[44] S. M. LaValle, *Planning algorithms*. Cambridge university press, 2006.

[45] M. M. Azari, S. Solanki, S. Chatzinotas, and M. Bennis, "Thz-Empowered UAVs in 6G: Opportunities, Challenges, and Trade-offs," *IEEE Commun. Magazine*, vol. 60, no. 5, pp. 24–30, 2022.

[46] H. Chen, H. Sarieddeen, T. Ballal *et al.*, "A Tutorial on Terahertz-Band Localization for 6G Communication Systems," *IEEE Commun. Surveys Tut.*, 2022.

[47] C. A. Balanis, *Antenna theory: analysis and design*. John wiley & sons, 2015.

[48] G. Fontanesi, A. Zhu, and H. Ahmadi, "Outage Analysis for Millimeter-Wave Fronthaul Link of UAV-Aided Wireless Networks," *IEEE Access*, vol. 8, pp. 111 693–111 706, 2020.

[49] D. R. Fuhrmann and G. San Antonio, "Transmit Beamforming for MIMO Radar Systems Using Signal Cross-Correlation," *IEEE Trans. Aerosp. Electron. Syst.*, vol. 44, no. 1, pp. 171–186, 2008.

[50] X. Liu, T. Huang, N. Shlezinger *et al.*, "Joint Transmit Beamforming for Multiuser MIMO Communications and MIMO Radar," *IEEE Trans. Signal Process.*, vol. 68, pp. 3929–3944, 2020.

[51] Y.-J. Chen and D.-Y. Huang, "Joint Trajectory Design and BS Association for Cellular-Connected UAV: An Imitation-Augmented Deep Reinforcement Learning Approach," *IEEE Internet Things J.*, vol. 9, no. 4, pp. 2843–2858, 2021.

[52] J. A. Vásquez-Peralvo, J. Querol, F. Ortíz *et al.*, "Flexible beamforming for direct radiating arrays in satellite communications," *IEEE Access*, 2023.

[53] N. Shlezinger, Y. C. Eldar, and S. P. Boyd, "Model-based deep learning: On the intersection of deep learning and optimization," *IEEE Access*, vol. 10, pp. 115 384–115 398, 2022.

[54] P. J. Freire, S. Srivallapanondh, A. Napoli, J. E. Prilepsky, and S. K. Turitsyn, "Computational complexity evaluation of neural network applications in signal processing," *arXiv preprint arXiv:2206.12191*, 2022.